Journal of Fluids and Structures (2002) **16**(8), 1073–1092
doi:10.1006/jfls.2002.0458 available online at http://www.idealibrary.com on IDEAL®

SUPPRESSION OF FLUID FORCES ACTING ON TWO SQUARE PRISMS IN A TANDEM ARRANGEMENT BY PASSIVE CONTROL OF FLOW

MD. MAHBUB ALAM, M. MORIYA, K. TAKAI AND H. SAKAMOTO

Department of Mechanical Engineering, Kitami Institute of Technology Kitami 090-8507, Japan

(Received 10 April 2000; and in final form 9 October 2001)

The suppression of fluid forces acting on two square prisms in a tandem arrangement in which a flow approaching the upstream prism was controlled by a thin flat plate was examined, with variation in spacing between the plate and the upstream prism. The width of the plate was one-ninth of the prism width. The position of the control plate was varied from the front surface of the upstream prism to 2·25 times the prism width in the upstream direction, and the position of the downstream prism was varied from the rear surface of the upstream prism to 10 times the prism width in the downstream direction. A dramatic decrease in fluid forces acting on both prisms was observed for a certain range of control plate positions. For such optimum positions of the control plate, the shear layers that separated from the control plate attached near the edges of the front surface of the upstream prism and each shear layer bifurcated into two layers, one part of the shear layers making a quasi-steady recirculating region between the control plate and the upstream prism, and the other part separating from the leading edges and attaching again to the side-surfaces of the upstream prism. When the control plate was placed with spacings $S/W = 1{\cdot}50 \sim 1{\cdot}90$ (S: spacing between the control plate and the upstream prism, W: width of the prism), the above-mentioned flow pattern appeared, and the fluid forces and vortex shedding of the upstream prism were almost completely suppressed. Also, the upstream prism was found to be insensitive to the existence of the downstream prism when the latter was located downstream, approximately six or more times the prism width.

1. INTRODUCTION

MANY ATTEMPTS have been made to suppress fluid forces acting on circular-, rectangular-, and square-sectioned models, and many methods for suppressing fluid forces acting on such models have been developed. Bearman (1965) attempted to reduce fluid forces as well as vortex shedding by fitting a splitter plate to the rear of a rectangular prism. Strykowski & Sreenivasan (1990) and Sakamoto *et al.* (1991) successfully suppressed vortex shedding by setting a control cylinder in a separated shear layer on one side of a circular cylinder and a square prism, respectively. Lesage & Gartshore (1987) and Igarashi & Itoh (1993) reduced time-averaged drag force by setting a small rod upstream of a square prism and, most recently, Sakamoto *et al.* (1997) evaluated the fluid forces acting on a square prism by changing the width of a flat plate and its position on the center-line. They found that the optimum width of the plate for suppression of fluid forces is approximately 1/10 of that of the prism.

0889-9746/02/081073 + 20 $35.00/0

The notable features of the flow over two bodies in a tandem arrangement are intensification of aerodynamic forces and unexpected vibration of the bodies. The fluid forces acting on the bodies change dramatically with changes in the spacing between them. Such an arrangement of two bodies has many practical applications in various fields of engineering, such as twin-conductor transmission lines, two parallel suspension bridges, radar mast vibrations, twin chimney stacks, heat exchanger tubes, and various structures on land and in the ocean.

Zdravkovich (1977) investigated the interference between two equal circular cylinders in a tandem arrangement, a side-by-side arrangement and a staggered arrangement, and he reported that there is a discontinuous change in the flow pattern and fluid forces acting on the cylinders at some critical spacing, where two types of flow pattern produce two values of force and the two patterns intermittently switch. Moriya & Sakamoto (1986) experimentally studied the flow around two circular cylinders in a tandem arrangement at a Reynolds number of $6{\cdot}54 \times 10^4$, in which the upstream prism is forcibly vibrated transversely with a vortex shedding frequency near that of the vortex shedding from the cylinder at rest. They concluded that the critical spacing between the cylinders for the flow to be switched from reattachment flow to jump flow is 2 times the cylinder diameter, and that the critical spacing is 2·5 times the cylinder diameter when both cylinders are at rest. Wind tunnel experiments were conducted on two square prisms in a tandem arrangement by Sakamoto *et al.* (1987) to determine the characteristics of flow and the behavior of time-averaged and fluctuating fluid forces. Thus, a number of previous studies have shown that there exists a critical spacing, at which discontinuity of fluid forces occurs due to change from one stable flow pattern to another, when two bodies are in a tandem arrangement. This change in the flow pattern creates large aerodynamic forces acting on the bodies. However, there have been no studies on suppression of fluid forces acting on two bodies in a tandem arrangement or on the jump phenomenon, which intensifies the fluid forces.

Hence, the aim of the present work was to find a way to suppress the fluid forces and the discontinuity of fluid forces acting on two two-dimensional square prisms in a tandem arrangement, which is regarded as the most fundamental arrangement. In order to achieve this aim, the approaching flow on an upstream prism was controlled to change the behavior of shear layers by placing a control plate centrally in front of the upstream prism. Time-averaged (steady) and fluctuating fluid forces acting on the two prisms were examined to determine the amount of reduction and to determine the optimum position of the control plate. In addition, the mechanism of flow control, structure of the controlled wake, and behavior of the controlled surrounding flow were investigated in detail on the basis of surface pressure distributions, vortex shedding frequency and visualized surface oil-flow patterns.

2. EXPERIMENTAL ARRANGEMENT AND PROCEDURES

The experiments were performed in a low-speed, closed-circuit wind tunnel. The test-section of the tunnel was rectangular, with a height of 0·6 m, width of 0·4 m and length of 5·4 m. Two types of square prism were used for the experiments: one with a load cell inside for the measurement of fluid forces, and the other with a semiconductor pressure transducer inside for the measurement of time-averaged and fluctuating pressure. Both prisms had a width of 42 mm and length of 400 mm, spanning the width of the test-section of the wind tunnel. As shown in Figure 1, the prism for the measurement of fluid forces was composed of two parts: an active prism (“live” section) and a dummy prism; a load

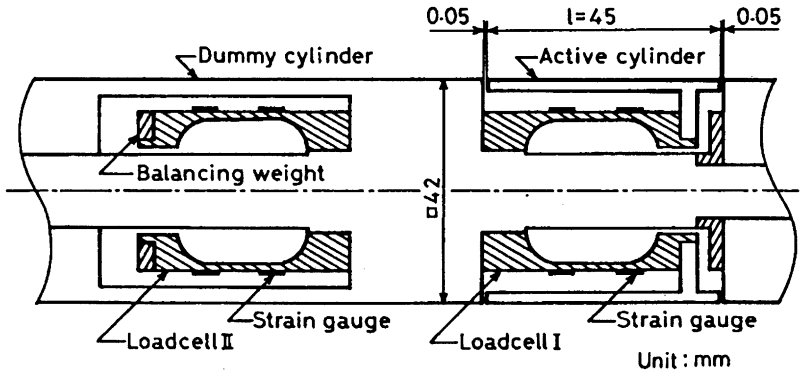

Fig. 1. Arrangement of load cells installed inside a square prism.

cell on which four semiconductor strain gauges had been installed was set inside each prism. The gap between the active and dummy prisms was set at 0·05 mm. The load cell installed inside the active prism measured a combination of fluid forces and force due to vibration transmitted from the outside through the prism support. The load cell installed inside the dummy prism measured forces due to vibration transmitted from the outside through the prism support. Hence, the fluid forces acting on the active prism could be calculated by subtracting the output of the load cell installed inside the dummy prism from that of the load cell installed inside the active prism. According to Savkar & So (1978), a natural frequency of at least 4 times that of the dominant force frequency is required for the measurement system to work with reasonable accuracy. The natural frequency of load cell I ('live' section) set in the active prism was about 1050 Hz, which is sufficiently high to satisfy the above condition.

To measure the surface pressure, a semiconductor pressure transducer (Toyoda DD102A) with a range of $\pm$ 10 kPa was used, and the transducer output was calibrated to give a reading of 12 V for 2 kPa of applied pressure. The pressure transducer responded to pressure fluctuation of up to 400 Hz with a gain factor of $1 \pm 0{\cdot}08$, the phase lag being negligible. This frequency was well above the frequency of vortex shedding from the prisms.

The control flat plate, made of stainless steel, was 5 mm in width and 0·2 mm in thickness. It was set in tension on the center-line of the front face of the upstream prism in a tandem arrangement as shown in Figure 2. No vibration of the control plate was generated during the experiment. All measurements were carried out with models suspended in a free-stream with turbulent intensity of 0·19%. The cylinders were rigidly clamped to steel square-sectioned bars attached to the walls of the tunnel. No end plates were used inside the wind tunnel walls because measurement of the span-wise velocity distribution showed that the thickness of the boundary layer of the approaching flow was very small.

Surface oil-film techniques were used to investigate the flow pattern on the prisms. A mixture composed of silicone oil, titanium dioxide, oleic acid and kerosene with a ratio of 45:3:2:2 in weight was used for surface oil-flow visualization. A prism wrapped in a black film of 0·03 mm in thick was uniformly smeared with the mixture, and then the prism was placed inside the wind tunnel to obtain a surface oil-flow pattern on the prism. A digital camera was used to obtain images of the surface oil-flow patterns.

The free-stream velocity U_o was kept constant at $20 \pm 0{\cdot}02$ m/s (Reynolds number $\mathrm{Re} = 5{\cdot}6 \times 10^4$). The position of the control plate was varied from the front face of the

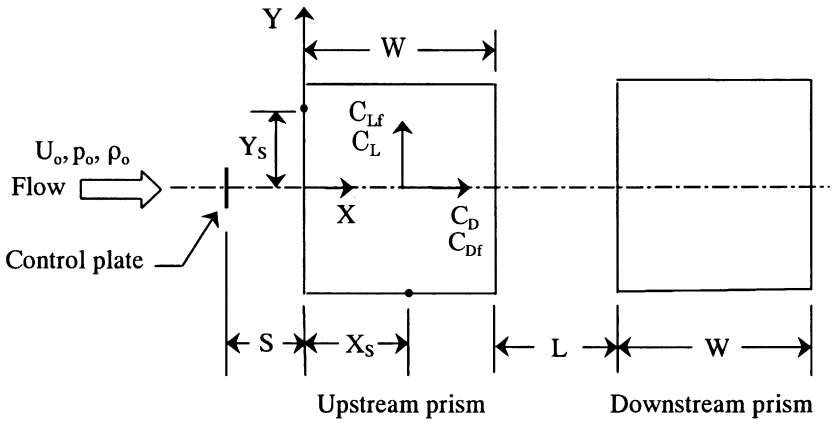

Fig. 2. Two prisms with a control plate in a tandem arrangement, showing also the coordinate system.

upstream prism to $S/W = 2{\cdot}25$ in the upstream direction along the center-line, and the position of the downstream prism was varied from the rear surface of the upstream prism to $L/W = 10$ in the downstream direction. The geometric blockage ratio and aspect ratio of the prism in the test-section were 7 and 9·52%, respectively. None of the results presented were corrected for the effects of wind-tunnel blockage.

3. RESULTS AND DISCUSSION

3.1. Control of Time-Averaged Pressure and Drag

Figure 3 shows the distribution of time-averaged pressure coefficients, C_p, on the surfaces of the upstream prism for control plate positions of $S/W = 0{\cdot}50$, $1{\cdot}75$, $2{\cdot}25$ and for no control at certain spacings, L/W. The figure shows that the pressure on the front surface of the upstream prism strongly depends on the positions of the control plate. In the case of $S/W = 0{\cdot}50$, the pressure is suppressed only over the central part of the front surface, and two symmetrical near-stagnation peaks exist. These peaks represent the reattachment of separated shear layers from the control plate onto the front surface of the upstream prism. For $S/W = 0{\cdot}50$ and $2{\cdot}25$, the pressure on the rear surface of the upstream prism with spacing $L/W = 4{\cdot}50$ is much lower in comparison with that in the case of no control. This is due to fact that when the control plate is positioned at those spacings, the rolling-up position of shear layers of the upstream prism recedes downward (Nakaguchi *et al.* 1968). In the case of $S/W = 1{\cdot}75$, the pressure distributions of the upstream prism with spacings $L/W = 3{\cdot}0$ and $4{\cdot}50$ are almost identical; that is, pressure on the surfaces of the upstream prism is not dependent on the spacing between the prisms. The pressure on all of the surfaces is considerably suppressed, and two small peaks are observed near the edges of the front surface.The existence of these two peaks on the front surface indicates that the shear layer separated from the control plate attaches to the front surface. The pressure distributions on the side surface indicate that the shear layer separated from the leading edge reattaches to the side surface.

The attachment of the shear layers to the front and side surfaces were confirmed by results obtained by using the surface oil-film technique. Photographs of surface oil-flow patterns on the front and side surfaces of the upstream prism are shown in Figure 4(a, b).

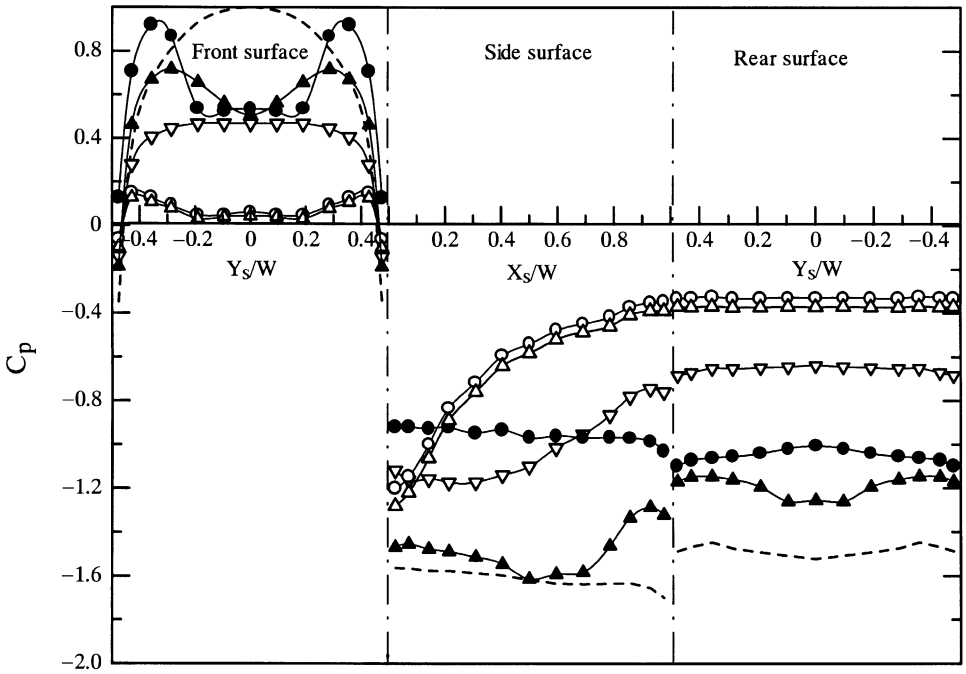

Fig. 3. Time-averaged pressure distribution along the surfaces of the upstream prism: ---, no control, $L/W = 4.50$; ●, $S/W = 0.50, L/W = 1.00$; ▲, $S/W = 0.50, L/W = 4.50$; ○, $S/W = 1.75, L/W = 3.00$; △, $S/W = 1.75, L/W = 4.50$; ▽, $S/W = 2.25, L/W = 4.50$.

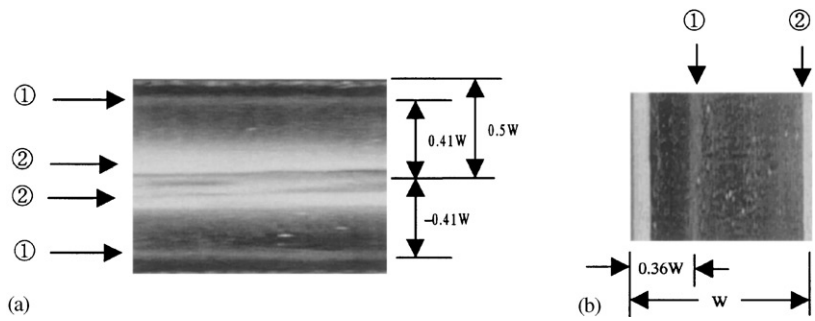

Fig. 4. Photographs of the surface oil-flow pattern of the upstream prism ($S/W = 1{\cdot}75$, $L/W = 4{\cdot}50$): ①, attachment line; ②, separation line. (a) Front surface; (b) Side surface.

In Figure 4(a), two reattachment lines marked by ① are seen on the front surface at $Y_s = \pm 0{\cdot}41$ W. The positions of these two reattachment lines coincide exactly with the positions of peaks in the pressure distribution on the front surface. The shear layer, having attached to the front surface, bifurcates into two shear layers, in which the inner part separates again at the line marked by ②. Conversely, the outer part of the shear layer separates from the leading edge and attaches again to the side surface at $X_s = 0{\cdot}36$ W

[Figure 4(b)]. The straightness and symmetry of reattachment lines indicate that the flow has good two dimensionality.

The distributions of time-averaged pressure coefficients, C_p, on the surfaces of the downstream prism for the control plate positions of $S/W = 0{\cdot}50$, $1{\cdot}75$, $2{\cdot}25$ and for no control are shown in Figure 5. It is noteworthy that, for $S/W = 0{\cdot}50$, $1{\cdot}75$ and $2{\cdot}25$ with $L/W = 4{\cdot}50$, the pressure coefficients on the front surface of the downstream prism are almost identical and are much larger than that in the case of no control with the same spacing. For small spacing between the prisms, e.g., $L/W = 1{\cdot}00$, the pressure on the front surface of the downstream prism for $S/W = 0{\cdot}50$ is negative and higher than that of the rear surface. In this position, the shear layers that separate from the upstream prism reattach to the side surfaces of the downstream prism and form a quasi-steady vortex region between them.

The variation of time-averaged drag coefficient, C_D, of the upstream and the downstream prisms with respect to the spacing ratio, L/W, is shown in Figure 6 for the control plate positions of $S/W = 0{\cdot}50$, $1{\cdot}50$, $1{\cdot}75$, $1{\cdot}90$, $2{\cdot}25$ and for no control. The drag coefficients of the upstream prism are suppressed for all control plate positions compared with that for prisms with no control. From Figure 6(a), it is evident that most of the suppression of fluid forces occurs when the control plate is located with spacings $S/W = 1{\cdot}50 \sim 1{\cdot}90$. In this range of control plate positions, the reduction in the time-averaged drag coefficient of the upstream prism is 84%. Also, for all of the controlled cases, the value of C_D of the upstream prism is almost independent of the position of the downstream prism. In the case of the downstream prism, there is a suppression of the drag coefficient for the control plate positions of $S/W = 1{\cdot}50 \sim 1{\cdot}90$ for spacings $L/W \leqslant 5{\cdot}5$, and the maximum reduction is 66%. Also, in this range of control plate positions, variation in the drag coefficient of the downstream prism is continuous; i.e., the jump

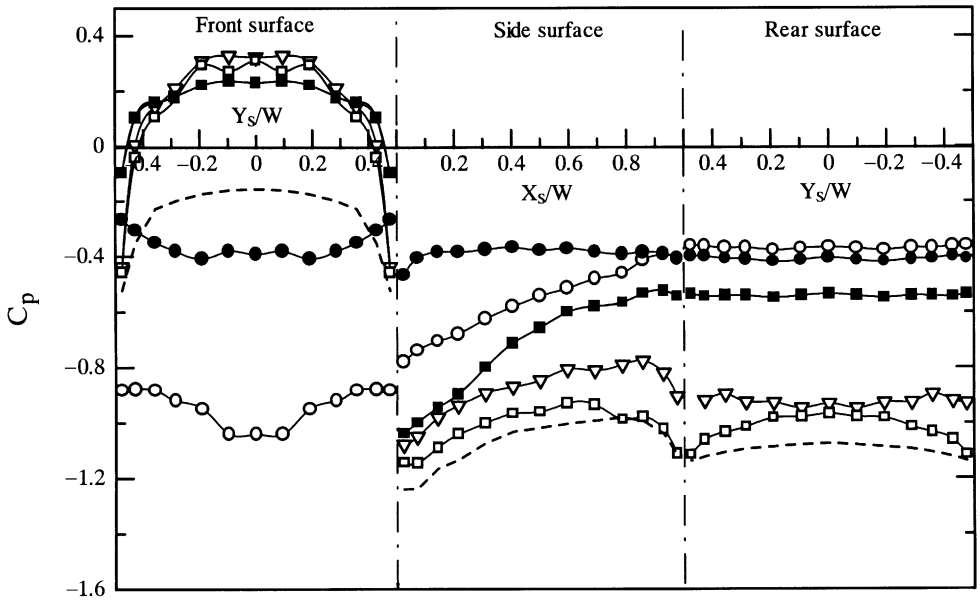

Fig. 5. Time-averaged pressure distribution along the surfaces of the downstream prism: ———, no control, $L/W = 4.50$; ○, $S/W = 0.50$, $L/W = 1.00$; □, $S/W = 0.50$, $L/W = 4.50$; ●, $S/W = 1.75$, $L/W = 1.00$; ■, $S/W = 1.75$, $L/W = 4.50$; ▽, $S/W = 2.25$, $L/W = 4.50$.

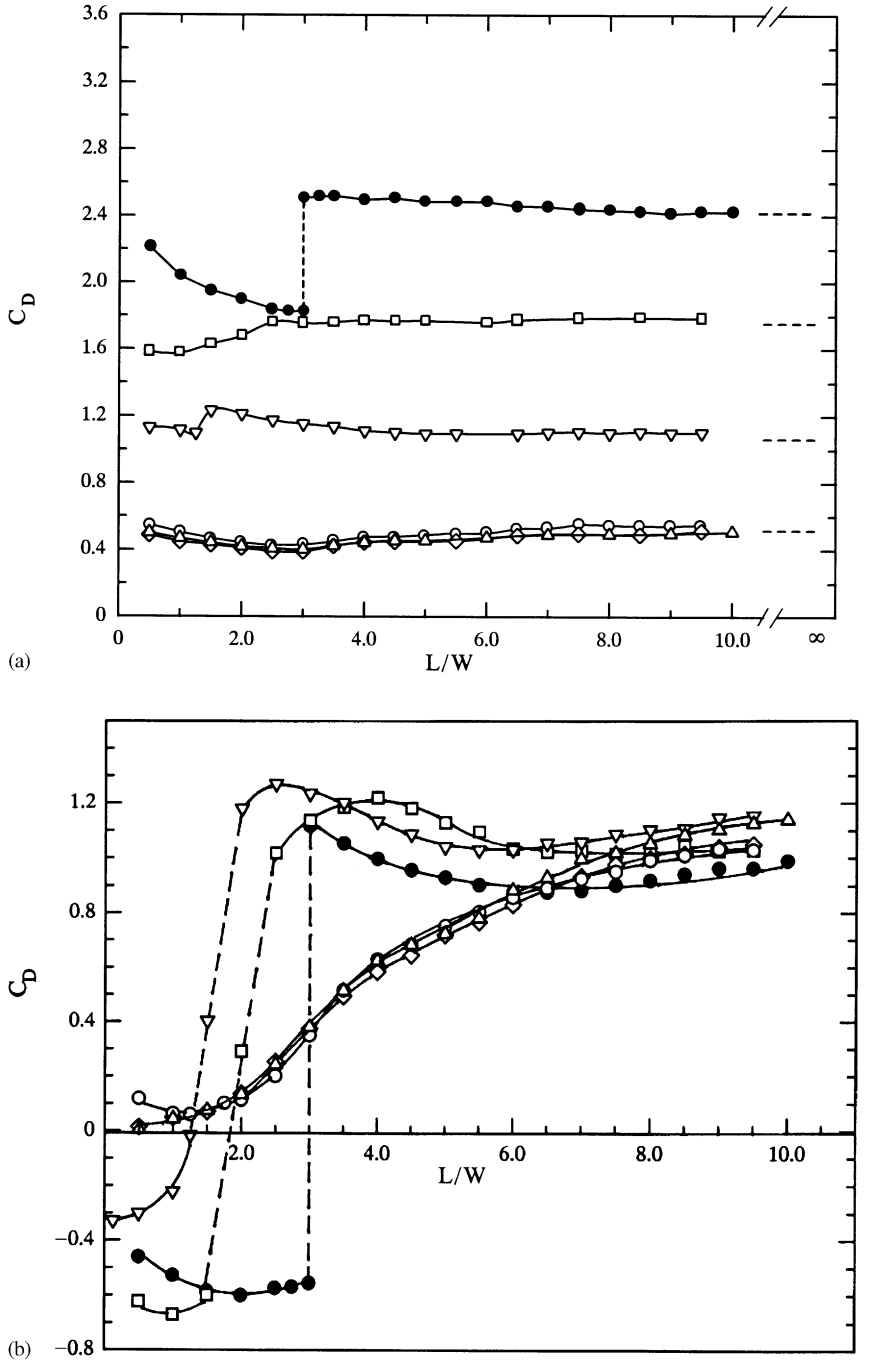

Fig. 6. Variation in time-averaged drag coefficient C_D with changes in spacing ratio L/W: (a) upstream prism; (b) downstream prism: ●, no control; □, S/W = 0.50; ○, S/W = 1.50; △, S/W = 1.75; ◇, S/W = 1.90; ▽, S/W = 2.25; – – –, single prism.

phenomenon in which a bistable flow appears intermittently is perfectly suppressed, while for the other cases, the distributions of drag coefficients show discontinuities that are indicative of the existence of bistable flow patterns.

For $S/W = 0{\cdot}50$ and 2·25, the effect of the jump phenomenon on C_D of the upstream prism is very small, but the effect on C_D of the downstream prism is still strong. In order to investigate the contributions of the front and rear surface pressures to the drastic change in C_D of the downstream prism, the averaged pressure coefficients, C_{pa} (see Appendix for definition), on these surfaces were evaluated from the pressure distributions. Figure 7 shows the average pressure coefficient of the front and rear surfaces of the downstream prism. The average pressure coefficient on the base surface increases suddenly to a maximum value and then decreases with increase in spacing between the prisms, while the average pressure coefficient on the front surface increases gradually. Based on these results, it is concluded that the effect of the jump phenomenon on C_D of the downstream prism is mostly bestowed from the wake of the downstream prism rather than from the wake formed by the upstream prism. Also, for $S/W = 1{\cdot}75$, the average pressure on the front and base surfaces increases and decreases, respectively, in a linear manner; therefore, the jump phenomenon does not occur in this case.

Next, we discuss the drag of the control plate. As an example, the drag coefficient of the control plate is 0·071 for the position of $S/W = 1{\cdot}75$, in which the drag force of the upstream prism is remarkably reduced. The drag coefficient of the control plate is estimated on the basis of the free-streamline theory proposed by Parkinson & Jandali (1970) by measuring the base pressure of the control plate. Thus, the drag of the control plate is significantly smaller than that of the upstream prism.

3.2. Control of Fluctuating Force

Figure 8 shows the distribution of r.m.s. pressure coefficients along the surfaces of the upstream and downstream prisms for certain spacings. In Figure 8(a), the fluctuating pressures on the side and rear surfaces of the upstream prism for $S/W = 2{\cdot}25$ are very sensitive to the spacing between the prisms, L/W. As the spacing increases from $L/W =$ 1·50 to 4·50, the pressure fluctuations on the side surfaces greatly decrease. The pressure

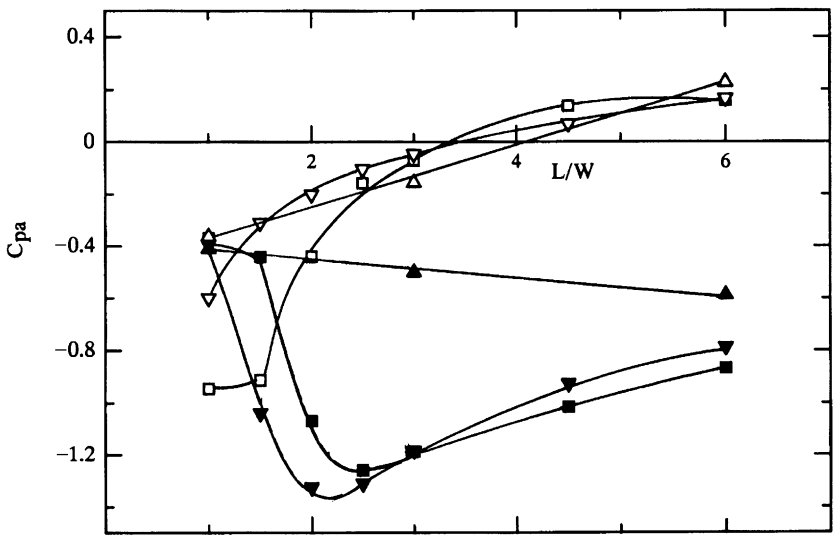

Fig. 7. Variation in average pressure on the surfaces of the downstream prism against spacing ratio L/W: □, $S/W = 0.50$, front surface; ■, $S/W = 0.50$, rear surface; △, $S/W = 1.75$, front surface; ▲, $S/W = 1.75$, rear surface; ▽, $S/W = 2.25$, front surface; ▼, $S/W = 2.25$, rear surface.

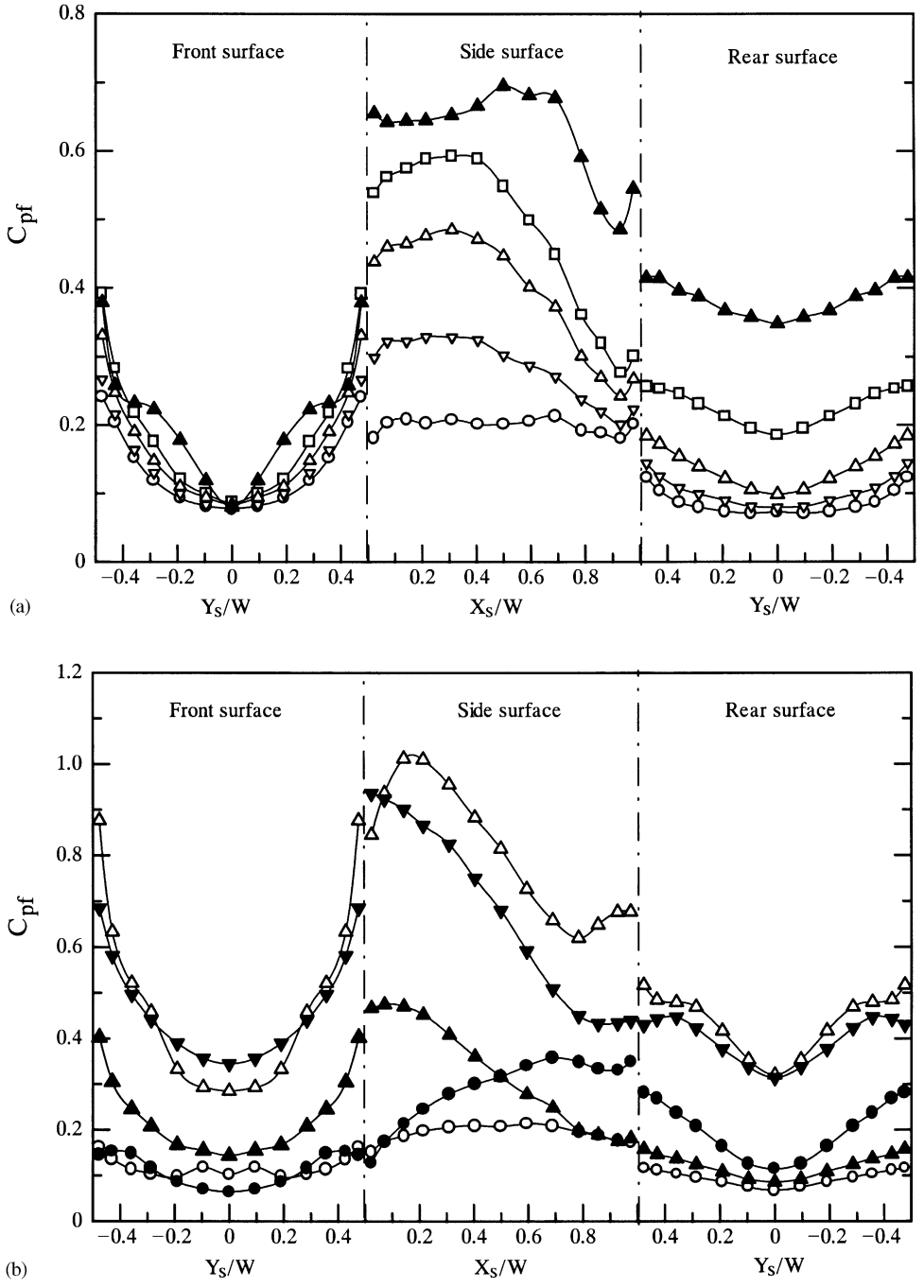

Fig. 8. Distribution of r.m.s. pressure coefficient C_{pf} along the surfaces of prisms. (a) Upstream prism: ▲, $S/W = 0.50$, $L/W = 4.50$; ○, $S/W = 2.25$, $L/W = 1.00$; □, $S/W = 2.25$, $L/W = 1.50$; △, $S/W = 2.25$, $L/W = 3.00$; ▽, $S/W = 2.25$, $L/W = 4.50$. (b) Downstream prism: ●, no control, $L/W = 1.00$; ▼, no control, $L/W = 4.50$; ○, $S/W = 0.50$, $L/W = 1.00$; △, $S/W = 0.50$, $L/W = 4.50$; ▲, $S/W = 1.75$, $L/W = 4.50$.

fluctuations on the rear surface for $S/W = 2{\cdot}25$ are much lower than those for $S/W = 0{\cdot}50$. This is because the vortex-formation region in the former case is farther behind than that in the latter case. For the downstream prism, the fluctuating pressures on the front and rear surfaces for $S/W = 1{\cdot}75$ with spacing of $L/W = 4{\cdot}50$ are much smaller than those for $S/W = 0{\cdot}50$ and for no control. For $S/W = 0{\cdot}50$ and no control, the profiles of pressure fluctuations on the side surfaces suggest that the shear layers that separated from the leading edges reattach intermittently to the side surfaces, since it is well known that the peak value of C_{pf} occurs somewhat upstream of the reattachment (Hiller & Cherry 1981). By comparing profiles and magnitudes of pressure fluctuations on the side and rear surfaces for $S/W = 0{\cdot}50$ and for no control with spacing $L/W = 1{\cdot}00$, it was determined that a von Karman type vortex appears behind the downstream prism in the case of no control and that no appreciable vortex appears behind the downstream prism in the case of $S/W = 0{\cdot}50$.

Figure 9 shows the trends in variation of the fluctuating drag coefficients, C_{Df}, on the upstream and downstream prisms with variation in L/W. The fluctuating drag coefficient of the upstream prism is suppressed by 25, 71 and 50% for $S/W = 0{\cdot}50$, $1{\cdot}50 \sim 1{\cdot}90$ and $2{\cdot}25$, respectively, compared with that in the case of no control for spacings $L/W \geqslant 3$. For the downstream prism positions at which the shear layers separated from the upstream prism and reattached to the downstream prism, the fluctuating drag coefficients of the upstream prism for the controlled cases are slightly larger than those for the no control. At these positions, the fluctuations of pressure on the rear surface of the upstream prism for all cases are almost the same, but greater fluctuation of pressure on the front face of the upstream prism occurs due to disturbance created by the control plate. Thus, the fluctuating drag coefficients for the controlled cases are relatively large before their bistable flow spacings. When the two prisms individually generate vortices, the fluctuation of pressure on the rear surface of the upstream prism for the controlled cases is much smaller than that for no control. It is for this reason that the rolling-up position of shear layers of the upstream prism for $S/W = 0{\cdot}50$ and $2{\cdot}25$ is far from the rear surface and that no vortex appears for $S/W = 1{\cdot}50 \sim 1{\cdot}90$. Hence the fluctuating drag coefficients of the upstream prism are considerably diminished for $L/W > 3$. The fluctuating drag coefficient of the downstream prism is suppressed for the cases of $S/W = 1{\cdot}50 \sim 1{\cdot}90$ and $2{\cdot}25$. The fluctuating drag coefficient of the downstream prism shows much larger values than that of the upstream prism. This is due to the fact that the downstream prism is situated in an approaching flow with strong turbulence intensity created by the upstream prism and the control plate. Therefore, the fluctuating drag is not only altered by fluctuation of the flow around the body caused by the vortices behind it but also greatly altered by the turbulence intensity of the approaching flow.

Figure 10 shows the measured values of the fluctuating lift coefficient, C_{Lf}, of the upstream prism, plotted against the spacing ratio L/W for each S/W. The maximum reductions in C_{Lf} of the upstream prism are 94 and 78% for $S/W = 1{\cdot}50 \sim 1{\cdot}90$ and $2{\cdot}25$, respectively, in comparison with that for no control. For the control plate position of $S/W = 2{\cdot}25$, the value of lift coefficient of the upstream prism is very small when the downstream prism is placed with spacings of $\mathrm{L/W} \geqslant 6$. This is because the position of the vortex region is further downstream from the upstream prism and narrow wake, since the strength of the vortex decreases as the vortex forms further away from the rear surface (Griffin & Ramberg 1974; Bearman & Trueman 1972). It is notable that, for $S/W = 2{\cdot}25$, the value of fluctuating lift coefficient of the upstream prism at $L/W = 1{\cdot}50$ is maximum and 3 times larger than that without the influence of the downstream prism ($L/W \geqslant 6$). That is, the rate of decrement in the lift coefficient for $S/W = 2{\cdot}25$ is greater than that for $S/W = 0{\cdot}50$ and for no control. This trend indicates that when the downstream prism is

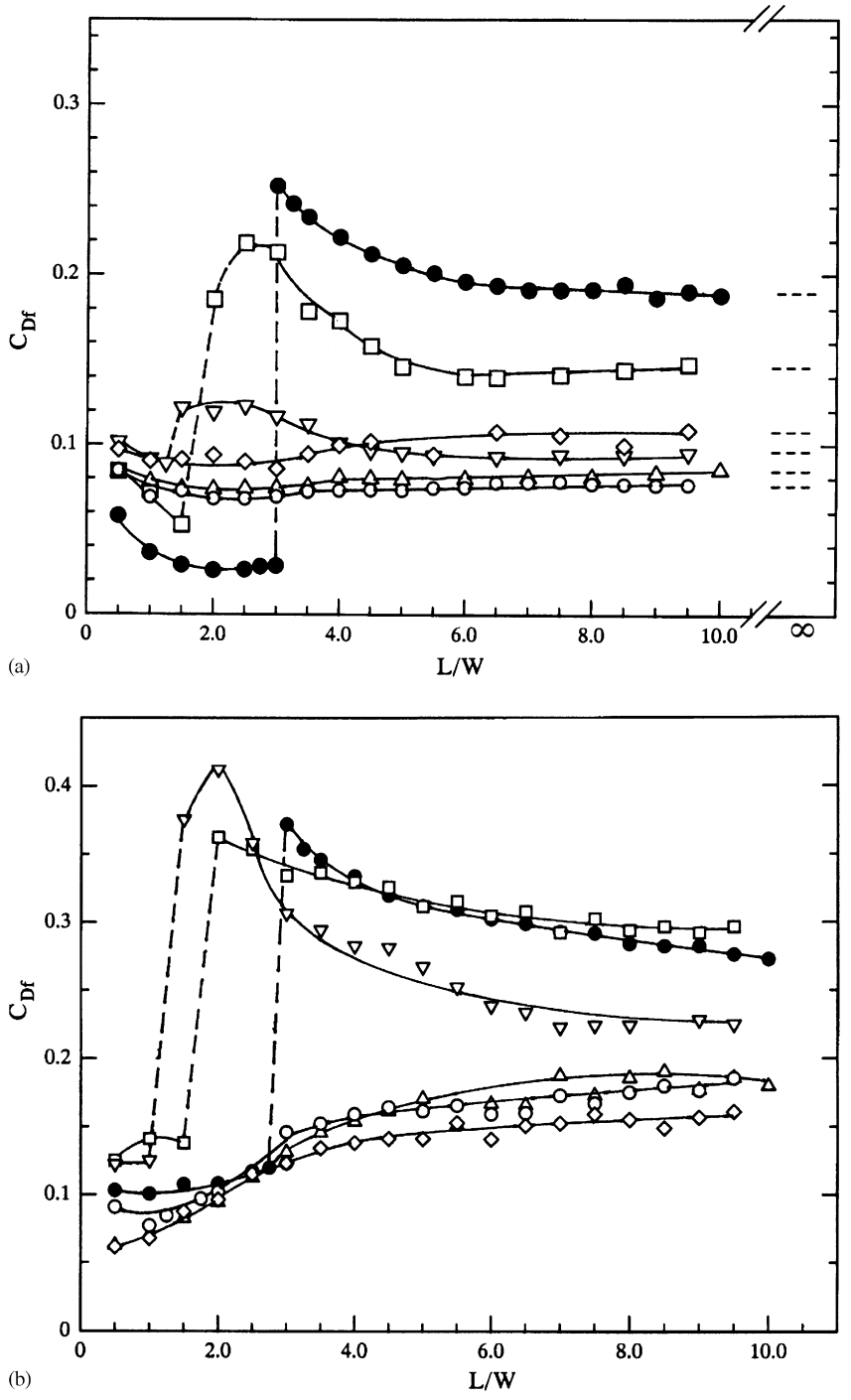

Fig. 9. Variation in r.m.s. fluctuating drag coefficient C_{Df} with changes in spacing ratio L/W for (a) upstream prism and (b) downstream prism: ●, no control; □, $S/W = 0.50$; ○, $S/W = 1.50$; △, $S/W = 1.75$; ◇, $S/W = 1.90$; ▽, $S/W = 2.25$; – – –, single prism.

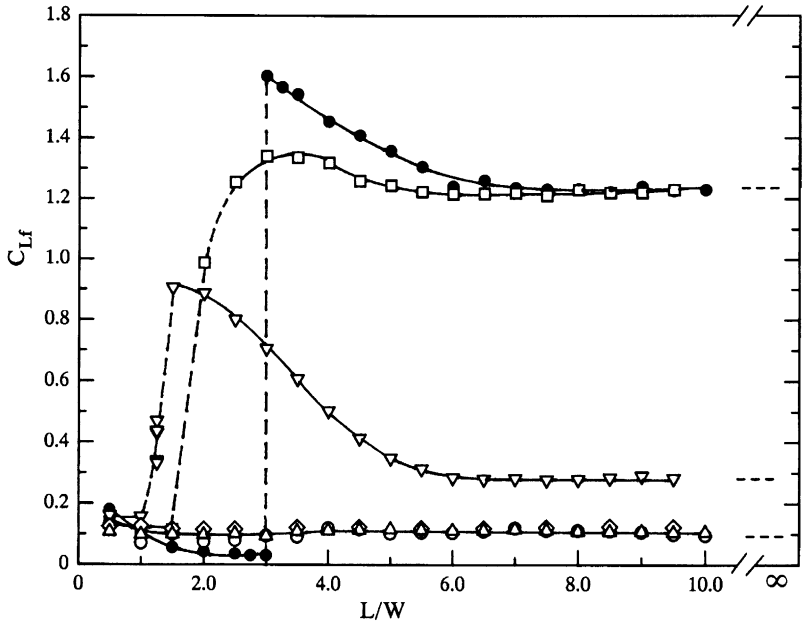

Fig. 10. Variation in fluctuating lift coefficient C_{Lf} of the upstream prism with changes in spacing ratio L/W for (a) upstream prism and (b) downstream prism: ●, no control; □, $S/W = 0.50$; ○, $S/W = 1.50$; △, $S/W = 1.75$; ◇, $S/W = 1.90$; ▽, $S/W = 2.25$; – – –, single prism.

set closer to the upstream prism from the spacing $L/W = 4{\cdot}50$ to 1·5, the shear layer rolls up strongly, with very regular periodicity, by moving the rolling-up position in the upstream direction.

In order to demonstrate the reliability of this phenomenon, the power spectrum distribution obtained from fluctuating lift force is shown in Figure 11. The spectrum distribution of the upstream prism shows that very sharp peaks indicative of orderly shedding of vortices appear for the range of spacing of $L/W = 1{\cdot}50 \sim 4{\cdot}50$ and that the peaks collapse to a very small magnitude for $L/W > 4{\cdot}50$. For $L/W > 4{\cdot}50$, the magnitude and width of the power spectrum peak are almost equal to that without a downstream prism ($L/W = \infty$). Therefore, the figure shows that the fluctuating lift force of the upstream prism is greatly influenced by the existence of the downstream prism within the range of spacings $L/W = 1{\cdot}50 \sim 4{\cdot}50$. In order to determine whether this is due to the feedback effect of the wake of the downstream prism or due to effect of the wake of the upstream prism, a third prism was added behind the downstream prism to exclude the effect of the wake of the downstream prism. The upstream prism was monitored to measure the fluctuating lift force and power spectrum. The measured fluctuating fluid forces and peak value of the power spectrum distribution of the upstream prism coincided with those in the case without a third prism. It therefore seems that this phenomenon is not dependent on the wake of the downstream prism. The peak of the power spectrum of the downstream prism also collapses to a small value when the downstream prism does not influence the upstream prism. Therefore, when perturbation of the shear layer of the upstream prism occurs due to the existence of the downstream prism, the shear layer over the downstream prism also becomes perturbed. The distribution of pressure fluctuations shown in Figure 8(a) also indicates the occurrence of the same phenomenon.

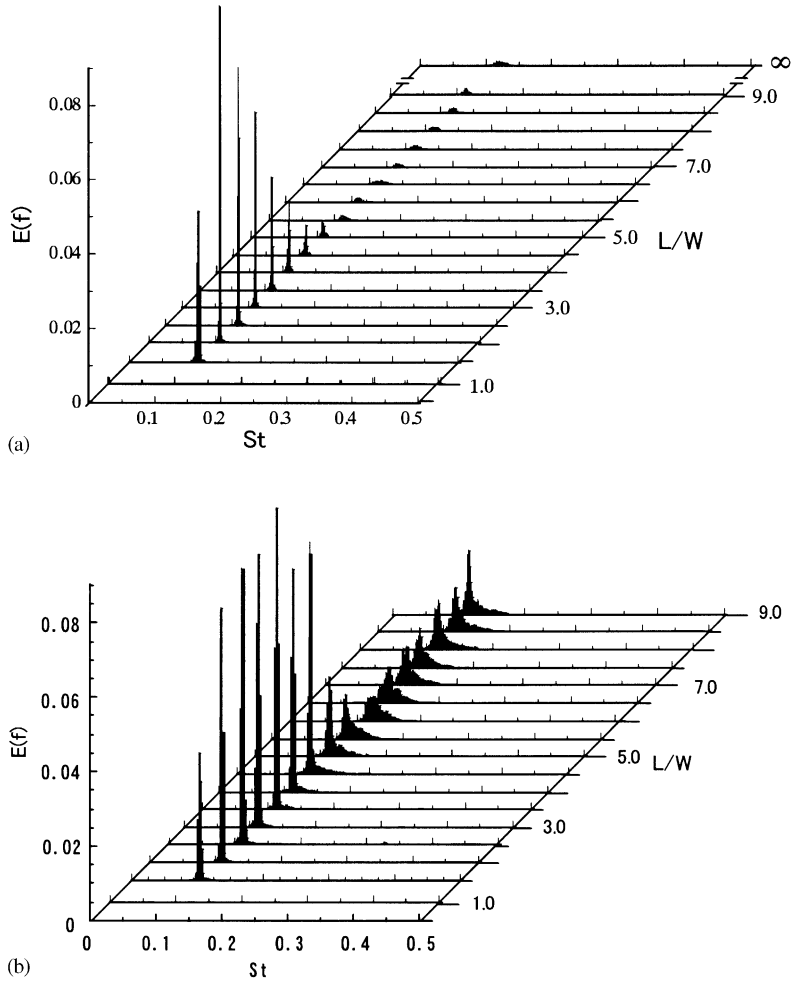

Fig. 11. Power spectrum from fluctuating lift forces acting on prisms against spacing ratio L/W ($S/W = 2.25$): (a) upstream prism; (b) downstream prism.

Figure 12 shows the measured values of fluctuating lift coefficient, C_{Lf}, of the downstream prism, plotted against the spacing ratio L/W for each S/W. For the no-control arrangement with spacing $L/W < 3$, the values of C_{Lf} of the downstream prism are larger than those of the upstream one. This is due to fact that the two prisms are connected by a quasi-steady vortex region between them, and clear vortices are formed only behind the downstream prism (Sakamoto *et al.* 1987). However, for spacings lower than those of bistable flow, the fluctuating lift coefficients of the downstream prism for the controlled cases are very small in comparison with those with no control. As the shear layers that separate from the upstream prism reattach almost steadily to the side surfaces of the downstream prism, periodic vortices do not form behind the downstream prism. Hence, for small spacings, fluctuating lift coefficients of the downstream prism for the controlled cases are smaller than those in the case of no control. The fluctuating lift coefficients for $S/W = 1{\cdot}50 \sim 1{\cdot}90$ are small and the jump phenomenon becomes negligible.

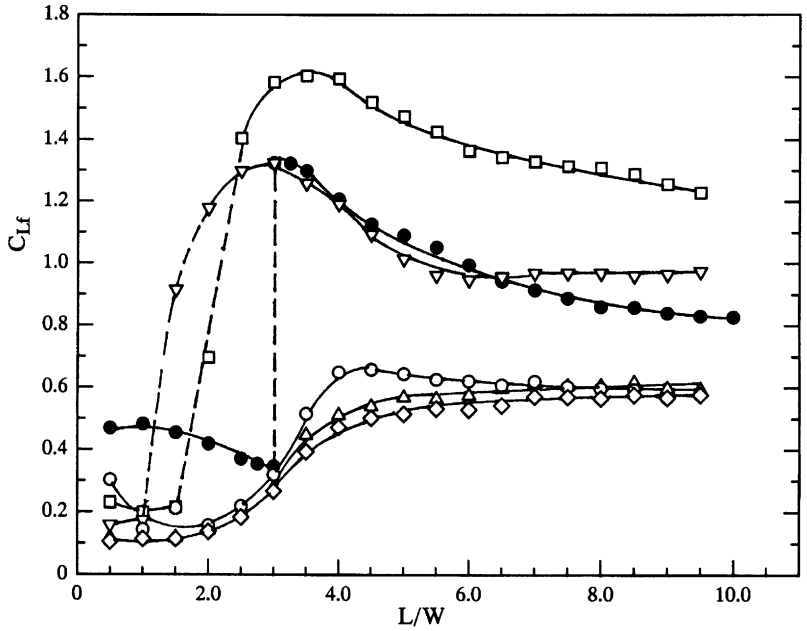

Fig. 12. Variation in fluctuating lift coefficient C_{Lf} of the downstream prism with changes in spacing ratio L/W for (a) upstream prism and (b) downstream prism: ●, no control; □, $S/W = 0.50$; ○, $S/W = 1.50$; △, $S/W = 1.75$; ◇, S/W = 1.90; ▽, $S/W = 2.25$; ---, single prism.

The jump of fluid forces is due to the presence of two flow patterns (bistable flow): (i) a reattachment flow, in which the shear layers that separate from the upstream prism reattache to the downstream prism and no periodic vortex is formed behind the upstream prism, and (ii) a detachment flow or jump flow, in which both prisms generate a von Karman type vortex behind them. The jump for the uncontrolled arrangement is very sharp and occurs at $L/W = 3{\cdot}0$, at which minimum and maximum values are seen for the first and second flow patterns, respectively. On the other hand, for the controlled cases, the jump of fluid forces is not so sharp; i.e., the jump phenomenon occurs in a wide range of spacings. Therefore, for the controlled cases, the bistable flow appears in a wide range of spacings and shifts toward lower values of L/W. It is reasonable to assume that as the wake of the upstream prism contracts due to turbulence somehow created by the control plate, the bistable flow shifts upstream. Sakamoto & Haniu (1988) examined the effects of turbulence on the fluid forces and the characteristics of bistable flow over two prisms in a tandem arrangement; they found that, as the addition of turbulence to a free stream causes the mean shear layer to thicken, bistable flow spacing shifts upstream and the bistable flow appears in a wide range of spacings.

Figures 6, 9 and 10 indicate that the upstream prism is almost insensitive to the position of the downstream prism when the downstream prism is positioned with $L/W \geqslant 6$. These figures show that there are no variations in C_D, C_{Lf} and C_{Df} of the upstream prism for any case when the spacings between the prisms are varied from $L/W = 6$ to 10, and that the values of these coefficients for $L/W \geqslant 6$ are equal to the values without a downstream prism ($L/W = \infty$). Thus, when the spacings between the prisms are $L/W \geqslant 6$, the upstream prism is completely insensitive to the existence of the downstream prism. At spacing of $L/W < 6$, the upstream prism is always influenced by the downstream prism.

3.3. Control of Vortex Shedding

The Strouhal number was calculated from the results of analysis of the power spectrum of the fluctuating lift force acting on the prism. Figure 13 shows the distribution of Strouhal numbers, St, for $S/W = 0{\cdot}50$, 1·50, 1·75, 1·90, 2·25 and for no control plotted against L/W. Vortex shedding behind the uncontrolled upstream prism appears only when spacings between the prisms are $L/W \geqslant 3$ and the frequency of the vortex shedding of the upstream prism (not shown) coincides with that of the downstream prism by synchronization. The results in the case of an uncontrolled downstream prism are in agreement with the results of Sakamoto *et al.* (1987), who calculated the vortex shedding frequency from the results of analysis of fluctuating pressure measured at the center of the side surface. For $S/W = 0{\cdot}50$ and 2·25, when the spacing between the prisms is small (i.e., spacing lower than bistable flow spacing), steady reattachments of the shear layers that separated from the upstream prism to the side surfaces of the downstream one occur, and no clear vortex can be found behind either prism; thus, Strouhal numbers are absent at these spacings. For $S/W = 0{\cdot}50$ and 2·25, a vortex behind each prism is formed for spacings of $L/W \geqslant 2{\cdot}0$ and $\geqslant 1{\cdot}50$, respectively. When a von Karman type vortex is shed

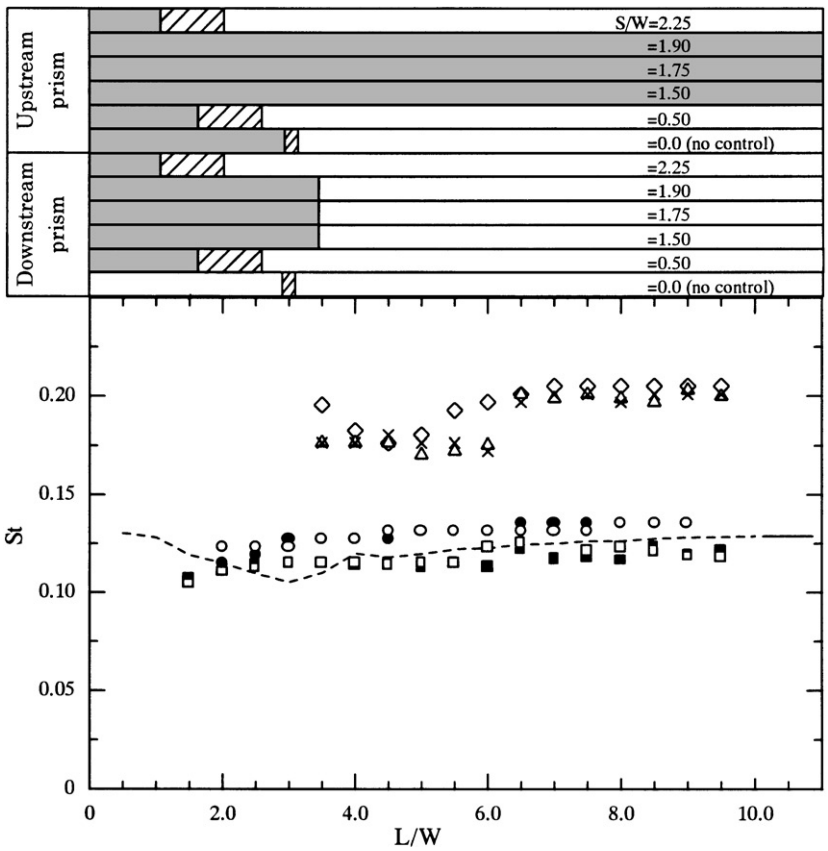

Fig. 13. Distribution of Strouhal numbers St including bistable flow, no vortex, and vortex region with changes in spacing ratio L/W: ---, downstream prism, no control; ●, upstream prism, $S/W = 0.50$; ○, downstream prism, $S/W = 0.50$; ◇, downstream prism, $S/W = 1.50$; △, downstream prism, $S/W = 1.75$; ×, downstream prism, $S/W = 1.90$; ■, upstream prism, $S/W = 2.25$; □, downstream prism, $S/W = 2.25$; —, single prism; ▨, bistable flow; ▭, no vortex; ▭, vortex region.

from the upstream prism, this triggers vortex shedding on the downstream prism; i.e., the frequency of the downstream prism is perfectly synchronized with the frequency of the upstream prism within the range tested.

For the control plate positions of $S/W = 1{\cdot}50 \sim 1{\cdot}90$, at which fluid forces are reduced significantly, the upstream prism does not generate any periodic vortices for any position of the downstream prism, and there is no bistable flow in this case. Within this range of control plate positions, the vortices behind the downstream prism are formed with a large Strouhal number for $L/W \geqslant 3{\cdot}5$. The figure also shows the range of bistable flow spacings, and the regions of vortex shedding and no vortex shedding, as a summary of vortex shedding.

3.4. Phase Lag of the Fluctuating Lift between the Two Prisms

Variations in the phase lag of the fluctuating lift between the two prisms are plotted against L/W for $S/W = 0{\cdot}50$, $2{\cdot}25$ and for no control in Figure 14. The phase lag is calculated from the cross-correlation between the fluctuating lift forces of the upstream prism, L_{fU}, and the downstream prism, L_{fD}, by

$$R_{L_{fU}L_{fD}}(\tau) = \frac{\overline{\{L_{fU}(t)\}\{L_{fD}(t+\tau)\}}}{\left[\overline{\{L_{fU}(t)\}^2}\right]^{\frac{1}{2}}\left[\overline{\{L_{fD}(t+\tau)\}^2}\right]^{\frac{1}{2}}},$$

where τ is the phase lag between the fluctuating lift forces of the prisms and t is the time. In this section, the phase lag of the fluctuating lift forces between two prisms is discussed for the spacings at which the vortices are shed periodically from each of the prisms. The phase lag of the fluctuating lift force between two prisms arising from vortex shedding depends on the distance between the two prisms, the vortex shedding frequency and the convective velocity. Figure 14 shows that the variations in phase lag of the lift forces of the two prisms

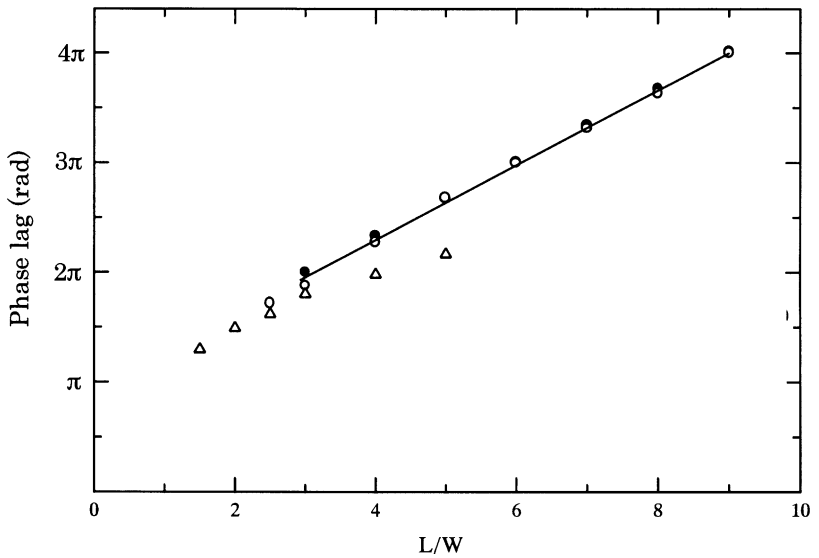

Fig. 14. Change in phase lag between fluctuating lift force of the upstream and downstream prisms with changes in spacing ratio L/W: ●, no control; ○, $S/W = 0.50$; △, S/W = 2.25; —, Sakamoto *et al.* (1987).

for no control and $S/W = 0{\cdot}50$ are the same and proportional to L/W. Also, the present results in the case of no control are the same as the results obtained by Sakamoto *et al.* (1987) for two prisms in a tandem arrangement. For the above cases, the lift forces on the two prisms are in phase, with phase lags of 2π and 4π, when the spacings between the prisms are $L/W = 3{\cdot}0$ and $9{\cdot}0$, respectively; they are out of phase, with a phase lag of 3π, for $L/W = 6{\cdot}0$. Similarly, the phase lag of fluctuating lifts for two circular cylinders in a tandem arrangement, the phase of the fluctuating lift of the downstream cylinder is delayed by 2π from that of the upstream cylinder at a spacing ratio of 2·8 and is delayed by another 2π at a spacing ratio of 6 (Sakata & Kiya 1983). Hence, it is clear that the vortex shedding frequency and convective velocity of these cases are different from each other. In the case of $S/W = 2{\cdot}25$, the phase lag commences from $L/W = 1{\cdot}50$ and ends at $L/W = 5{\cdot}0$. Beyond $L/W = 5{\cdot}0$, there is no distinct phase lag between the prisms.

3.5. Controlled Approaching Flow Pattern and Flow Pattern Over Two Prisms

The controlled approaching flow pattern and the flow pattern over two prisms for different positions of the control plate are described in what follows.

(i) *Case of* $S/W = 0{\cdot}50$. In this case, the shear layers that separate from the control plate reattach to the front surface of the upstream prism and each shear layer bifurcates into two shear layers. The inner parts of the shear layers deflect upstream and make a quasi-steady vortex region between the control plate and the upstream prism. The outer parts of the shear layers separate again from the leading edges and roll up behind the upstream prism for $L/W \geqslant 2{\cdot}5$ or reattach to the side surface of the downstream prism for $L/W \leqslant 1{\cdot}50$. Figure 15(a) shows sketches of flow patterns over the control plate and the prisms for $L/W = 4{\cdot}50$. The shear layers that separate from the leading edges of the downstream prism reattach intermittently to the side surfaces. When spacing between the

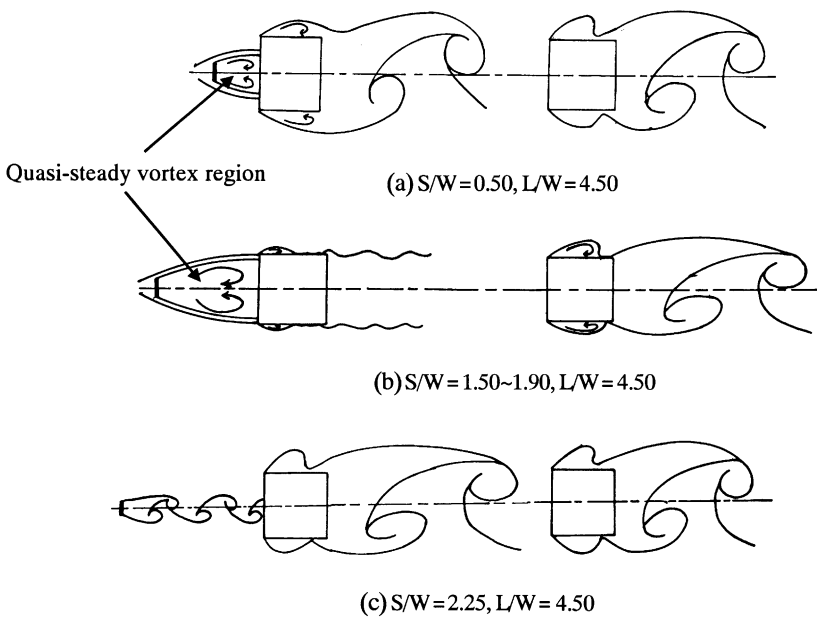

Fig. 15. Sketches of flow patterns based on fluid forces, surface oil-flow pattern, Strouhal number and pressure distribution.

prisms decreases from $L/W = 4{\cdot}50$ to $2{\cdot}50$, the enhancement of shear layers of each prism increases.

(ii) *Cases of* $S/W = 1{\cdot}50 \sim 1{\cdot}90$. When the control plate is positioned with spacing $S/W = 1{\cdot}50 \sim 1{\cdot}90$, the shear layers that separate from the control plate attach near the edges of the front face of the upstream prism in the same way as that in the case of $S/W = 0{\cdot}50$, but the difference is that the outer parts of the shear layers attach again permanently to the side surfaces of the same prism. Therefore, no appreciable vortex can be found behind the upstream prism. For the downstream prism, the shear layers reattach to the side surfaces (as confirmed by the surface oil-flow pattern) and generate periodic vortices behind it starting from $L/W = 3{\cdot}50$. The corresponding sketch of flow patterns is shown in Figure 15(b) for $L/W = 4{\cdot}50$.

(iii) *Case of* $S/W = 2{\cdot}25$. In this case, von Karman type vortex streets are formed behind the control plate [Figure 15(c)]. The shear layers separate from the leading edges of the upstream prism and reattach intermittently to the side surfaces. For $L/W \geqslant 4{\cdot}50$, the shear layers that separate from the upstream prism roll up weakly behind the rear surface, but as the spacing decreases, the shear layers roll strongly and the rolling position moves upstream. The flow over the downstream prism is almost the same as that for $S/W = 0{\cdot}50$.

3.6. Optimum Location of the Control Plate

Considering the suppression of fluid forces as well as vortex shedding, it can be concluded that most of the reduction in fluid forces as well as suppression of vortex shedding occurs at the control plate positions of the $S/W = 1{\cdot}50 \sim 1{\cdot}90$. At these positions of the control plate, the reduction in time-averaged drag, fluctuating lift and drag force of the upstream prism are 84, 94 and 71%, respectively. In this situation, the drag force of the downstream prism is suppressed for the spacing ratio of $L/W \leqslant 5{\cdot}5$, and the fluctuating lift and drag are significantly reduced in the range of spacings tested.

4. CONCLUSIONS

The objective of this work was to suppress the fluid forces and discontinuity of fluid forces acting on two square prisms in a tandem arrangement by controlling the approaching flow to the upstream prism by the use of a thin flat plate. The main results of the present work are summarized as follows.

(i) The maximum reduction in the time-averaged drag of the upstream prism occurs when the control plate is located at $S/W = 1{\cdot}50 \sim 1{\cdot}90$. The time-averaged drag is considerably reduced for the range of spacings $L/W = 0 \sim 10$ examined. Also, when the control plate is located at $S/W = 1{\cdot}50 - 1{\cdot}90$, the time-averaged drag of the downstream prism is suppressed for the spacing ratio of $L/W \leqslant 5{\cdot}5$. The maximum reductions in time-averaged drag are 84% for the upstream prism and 66% for the downstream prism.

(ii) The fluctuating lift and drag of the upstream prism are almost completely suppressed without the jump phenomenon when the control plate is located at $S/W = 1{\cdot}50 \sim 1{\cdot}90$. Also, the fluctuating lift and drag of the downstream prism are considerably diminished to a small value. The maximum reductions in fluctuating lift and drag are 94 and 71% for the upstream prism and 80 and 65% for the downstream prism, respectively.

(iii) Discontinuity is caused by an abrupt change from one stable flow pattern to another (the so-called bistable flow) when two square prisms without control are positioned in a tandem arrangement with the spacing $L/W = 3{\cdot}0$. A bistable flow appears in a wide range

of spacings and shifts toward lower values of L/W when the approaching flow is controlled by a plate, and the bistable flow disappears when the vortex shedding behind the upstream prism is completely suppressed. When the control plate is located upstream, $S/W = 1{\cdot}50 \sim 1{\cdot}90$, the jump phenomenon (bistable flow) is completely suppressed.

(iv) In all of the cases examined, the existence of the downstream prism influences the flow pattern of the upstream prism when the downstream prism is located with spacings $L/W < 6$. When the downstream prism is located with spacings $L/W \geqslant 6$, the upstream prism is completely insensitive to the existence of the downstream prism.

(v) When the shear layers that separate from the control plate reattach near the edges of the front face of the upstream prism, so that the inner parts of the shear layers make a quasi-steady vortex region between the control plate and the upstream prism and the outer parts of the shear layers attach again onto the side surfaces of the same prism, the greatest reductions in fluid forces occur. Also, the alternate vortex shedding behind the upstream prism is completely suppressed when this flow pattern appears.

APPENDIX: NOMENCLATURE

A	projected area of active section of prism
C_D	time-averaged drag coefficient, $C_D = D/(0.5\rho_o U_o^2 A)$
C_{Df}, C_{Lf}	r.m.s. (fluctuating) drag and lift coefficient of prism ($C_{Df}, C_{Lf} = \sqrt{\overline{D_f^2}}, \sqrt{\overline{L_f^2}}/(0.5\rho_o U_o^2 A)$)
C_p	time-averaged pressure coefficient, $C_p = (p - p_o)/(0.5\rho_o U_o^2)$
C_{pf}	r.m.s. (fluctuating) pressure coefficient, $C_{pf} = \sqrt{\overline{p_f^2}}/(0.5\rho_o U_o^2)$
C_{pa}	average pressure coefficient, $C_{pa} = \dfrac{\left\{\int_{-0.5W}^{0.5W} C_p dYs\right\}}{W}$
D	time-averaged drag force acting on the active prism
D_f, L_f	fluctuating drag and lift force acting on the active prism
f	frequency of vortex shedding
L	spacing between upstream and downstream prism (Figure 2)
p, p_f	time-averaged and fluctuating pressure acting on prism
$R_{L_{fu}L_{fD}}$	cross-correlation coefficient between fluctuating lift forces of upstream and downstream prism
S	spacing between control plate and upstream prism (Figure 2)
St	strouhal number of vortex shedding, $\mathrm{St} = fW/U_o$
t	time
U_o, p_o, ρ_o	velocity, static pressure and density of free-stream fluid
W	width of square prism (Figure 2)
X, Y	streamwise and lateral coordinate axis (Figure 2)
X_S, Y_S	position of piezometric hole on the surface of prism (Figure 2)
τ	phase lag

REFERENCES

BEARMAN, P. W. 1965 Investigation of flow behind a two-dimensional model with blunt trailing edge and fitted with splitter plates. *Journal of Fluid Mechanics* **21,** 241–255.

Bearman, P. W. & Trueman, D. M. 1972 An investigation of the flow around rectangular cylinders. *Aeronautical Quarterly* **23,** 229–237.

Griffin, M. & Ramberg, E. 1974 The vortex street wakes of vibrating cylinders. *Journal of Fluid Mechanics* **66,** 553–576.

Hilliier, R. & Cherry, N.J. 1981 The effects of stream turbulence on separation bubbles. *Journal of Wind Engineering & Industrial Aerodynamics* **8,** 49–58.

Igarashi, I. & Itoh, S. 1993 Drag reduction of a square prism (1st report, flow control around a square prism using a small vortex shedder). *ASME Journal of Fluids Engineering* **59,** 3701–3707.

Lesage, F. & Gartshore, I.S. 1987 A method of reducing drag and fluctuating side force on bluff bodies. *Journal of Wind Engineering & Industrial Aerodynamics* **25,** 229–245.

Moriya, M. & Sakamoto, H. 1986 Effect of a vibrating upstream cylinder on a stationary downstream cylinder. *ASME Journal of Fluids Engineering* **108,** 180–184.

Nakaguchi, H., Hasimoto, K. & Muto, S. 1968 An experimental study of aerodynamic drag on rectangular cylinders. *Journal of Japan Society of Aeronautical Space Science* **16,** 1–5.

Parkinson, G. V. & Jandali, T. 1970 A wake source model for bluff body potential flow. *Journal of Fluid Mechanics* **40,** 577–594.

Sakamoto, H. & Haniu, H. 1988 Effect of free stream turbulence on characteristics of fluctuating forces acting on two square prism in tandem arrangement. *ASME Journal of Fluids Engineering* **110,** 140–146.

Sakamoto, H., Haniu, H. & Obata, Y. 1987 Fluctuating forces acting on two square prisms in a tandem arrangement. *Journal of Wind Engineering & Industrial Aerodynamics* **26,** 85–103.

Sakamoto, H., Takeuchi, N., Haniu, H. & Tan, K. 1997 Suppression of fluid forces acting on square prism by passive control. *ASME Journal of Fluids Engineering* **119,** 506–511.

Sakamoto, H., Tan, K. & Haniu, H. 1991 An optimum suppression of fluid forces by controlling a shear layer separated from a square prism. *ASME Journal of Fluids Engineering* **113,** 183–189.

Sakata, I. & Kiya, M. 1983 Fluctuation acting on two circular cylinders in tandem arrangement. *Transactions of JSME* **49,** 2618–2623 (in Japanese).

Savkar, S. D. & So, R. M. C. 1978 On the buffeting response of a cylinder in a turbulent crossflow. TIS Report No. 78 CRD 119. Research and Development Center, General Electric Company.

Strykowski, P. J. & Sreenivasan, K. R. 1990 On the formation and suppression of vortex 'shedding' at low Reynolds numbers. *Journal of Fluid Mechanics* **218,** 71–107.

Zdravkovich, M.M. 1977 Review of flow interference between two circular cylinders in various arrangement. *ASME Journal of Fluids Engineering* **199,** 618–633.